



FLOWSTONES FROM THE RAČIŠKA PEČINA CAVE (SW SLOVENIA) RECORD 3.2-MA-LONG HISTORY

P. SIERPIEŃ*, J. PAWLAK, H. HERCMAN, P. PRUNER, N. ZUPAN HAJNA, A. MIHEVC, P. BOSÁK

Institute of Geological Sciences, Polish Academy of Sciences, ul. Twarda 51/55, PL-00-818 Warszawa, Poland
Institute of Geology of the Czech Academy of Sciences, Rozvojová 269, 165 00 Praha 6, Czech Republic
ZRC SAZU Karst Research Institute, Titov trg 2, 6230 Postojna, Slovenia

Received 07 October 2019 Accepted 12 February 2021

Abstract

Establishing a chronology of events is a critical step in reconstructing the palaeoclimate and it is important for all types of environmental records, including speleothems. Here, we analysed a unique series of flowstones deposited between 3.2 Ma (marine isotope stage (MIS) Km3) and 0.08 Ma (MIS 5). The studied flowstones are located in a classic karstic environment, the Račiška Pečina Cave in south-western Slovenia. Further, a detailed chronology of events was constructed based on oxygen isotope stratigraphy (OIS), combined with magnetostratigraphy and U-series dating. Two curves were selected as reference records where the LR04 record was used as the global curve and a Mediterranean record was used as the regional curve. The Račiška Pečina profile was divided into two segments separated by a principal disconformity. The lower segment correlated better with the regional Mediterranean curve, while the upper segment was with the global LR04 curve. These findings suggest that the main factors controlling environmental conditions in the cave area changed between 3.2 and 0.8 million years ago.

Keywords

stable isotopes, paleoclimate, OIS method, paleomagnetic data, Dinarides

1. Introduction

Speleothems are important terrestrial archives used for reconstructing paleoenvironmental conditions. The reliability of speleothem-derived data is a direct result of the close and well-known relationship between physico-chemical parameters (e.g. the isotopic compositions of C and O) and the conditions of speleothem crystallisation (e.g. McDermott, 2004; Lachniet, 2009; Fairchild and Baker, 2012). Additionally, it is possible to reliably date speleothems via U-series (e.g. Scholz and Hoffmann, 2008; Baker *et al.*, 2011; McDermott *et al.*, 2011) or paleomagnetic/magnetostratigraphic (e.g., Morinaga *et al.*, 1994; Lascu and Feinberg, 2011) dating methods. However, neither method is perfect. Uranium-series dating, like all physicochemical methods, is influenced by several limitations; in this case, the U concentration must be at a minimum level of few parts per million (Hellstrom, 2006; Fairchild and Baker, 2012), the admixture of detrital impurities must be as low

as possible, and the maximum age range of the method is ~700 ka (Cheng *et al.*, 2016).

Palaeomagnetism can provide only correlative ages and relies on the reconstruction of polarity changes in Earth's magnetic field; if these records are not calibrated with other methods of stratigraphic research, matching with the Geomagnetic Polarity Time Scale (GPTS; Cande and Kent, 1995) is difficult. The erosion or discontinuous deposition of cave sediments renders such correlations even more problematic as hiatal periods can hide substantial amounts of time (Bosák *et al.*, 2000, 2002, 2003; Zupan Hajna *et al.*, 2008, 2010, 2020). Therefore, the polarity changes located in hiatuses may not record the age as expected from the GPTS (Lascu and Feinberg, 2011). So oxygen isotope stratigraphy (OIS) was applied here to acquire a more detailed chronology of the speleothems examined. The analysis of the stable isotopic composition of oxygen is a standard method for tracking paleoclimatic changes in speleothems. The resultant oxygen curves can be used for correlation

Corresponding author: (P. Sierpień)
e-mail: paulasierpień@twarda.pan.pl

with a reference record that exhibits global or regional characteristics (Lisiecki and Raymo, 2005; Wang *et al.*, 2010).

Note that many speleothem studies are based on relatively young samples (e.g., Lauritzen and Lundberg, 1999; Vaks *et al.*, 2006; Affek *et al.*, 2014) and samples older than Pleistocene-age are rare (Vaks *et al.*, 2013). Cave sediments in the classical karstic Račiška Pečina Cave in SW Slovenia are a part of this rare category, having a total age range from 3.2 Ma to ~2 ka (Zupan Hajna *et al.*, 2021). They also contain well-developed and time-limited normal-polarised Olduvai Subchron ages (1.95–1.77 Ma) (Zupan Hajna *et al.*, 2008, 2010, 2020). The Pleistocene and Pliocene ages of the Račiška Pečina profile are interesting because of the climatic and paleogeographic changes that occurred on Earth's surface during these periods (Zacwijn, 1974; Van Couvering, 1996; Lourens *et al.*, 2004). The climate dried, steppisation occurred, and glacial development began, initially in the southern hemisphere and later in the north (Van Couvering, 1996; Gradstein *et al.*, 2012). Characteristic cycles of warm (interglacial) and cold (glacial) periods also began in the Pleistocene (Stanley, 2005).

Carbon and oxygen stable isotopes (expressed as $\delta^{13}\text{C}$ and $\delta^{18}\text{O}$ values, $\delta = \left(\frac{R_{\text{sample}}}{R_{\text{standard}}} - 1 \right)$, where R is the $^{13}\text{C}/^{12}\text{C}$ and $^{18}\text{O}/^{16}\text{O}$ ratio in the sample and the standard) represent the most frequently applied proxies for the reconstruction of paleoenvironmental conditions from speleothems (McDermott, 2004; Lachniet, 2009; Fairchild and Baker, 2012; Ünal-İmer *et al.*, 2016; Demeny *et al.*, 2017). The C and O isotope compositions in speleothem calcite are primarily controlled by the isotopic composition of the percolating water and the $\delta^{18}\text{O}$ of dripping water depends on the source of moisture, its transportation, the intensity of atmospheric precipitation and ambient air temperature. The oxygen isotope compositions of precipitation are altered by local conditions, such as temperature and the amount of precipitation at a given site (Lachniet, 2006; Lambert and Aharon, 2011; Fairchild and Baker, 2012). During the slow degassing of CO_2 and without evaporation, speleothem calcium carbonate crystallises near or in isotopic equilibrium with dripping water (Lauritzen and Lundberg, 1999) and as a function of the air temperature of the cave (Hendy, 1971).

Many studies have shown (e.g., Ayalon *et al.*, 2002; Levin *et al.*, 2009; Demeny *et al.*, 2017) that the $\delta^{18}\text{O}$ values of cave drip waters are constant over a long period of time and can nearly equal the oxygen isotope composition of the mean annual precipitation outside of the cave (e.g., Sundqvist, 2007). The temperature in a cave is also very close to the mean annual (surface) temperature in the region above the cave (Sundqvist, 2007; Fairchild and Baker, 2012). Carbon isotope compositions can provide information on climatic and vegetation conditions

(McDermott, 2004; McDermott *et al.*, 2006). The main factor controlling the $\delta^{13}\text{C}$ ($^{13}\text{C}/^{12}\text{C}$ ratio) of speleothem calcites are the proportions of CO_2 from organic sources and dissolved carbonate rocks (McDermott, 2004; Fohlmeister *et al.*, 2020). The C isotope composition of soil CO_2 is affected by the type of vegetation existing above a cave, which depends on photosynthetic pathways (C3 or C4 plants) and soil respiration rates (McDermott, 2004; Spötl *et al.*, 2016; Fohlmeister *et al.*, 2020). For C isotopes, the fractionation effect is temperature-dependent and is initiated by the dissolution of soil CO_2 in infiltrating meteoric water (Hendy, 1971). The main objectives of this study were to improve estimated speleothem chronologies based on OIS, which was tested as an alternative dating method, and to develop a regional paleoenvironmental interpretation of the obtained records (including the $\delta^{13}\text{C}$ and $\delta^{18}\text{O}$ records).

2. Geological Setting

The Račiška pečina Cave (RP) (45°30'N; 14°09'E; 609 m a.s.l.) (**Fig. 1A**) is located in the south-eastern part of the Matarsko Podolje, a part of the classical karstic terrain in SW Slovenia (Zupan Hajna *et al.*, 2008, 2010). The RP represents a paragenetic or epiphreatic relict cave, which is 304 m long, 10 m wide at maximum (Pruner *et al.*, 2003) and a simple south-dipping gallery (Bosák *et al.*, 2004). It is part of an old cave system, which was partly opened to the surface by denudation (Zupan Hajna *et al.*, 2008). The cave formed in thickly bedded limestones, dolomites and breccias of Lower Cretaceous period (Šikič *et al.*, 1972). Allogenic siliciclastic sediments, primarily clays and sands of unknown thicknesses that fill the lower part of the cave, are covered by various layered speleothems (Pruner *et al.*, 2003). A 13-m-long profile through clearly stratified speleothems intercalated by muds is situated in the southern part of the cave, approximately 200 m from the present entrance (**Fig. 1B**). The primary thickness of the studied section reaches 223 cm (Horáček *et al.*, 2007; Zupan Hajna *et al.*, 2008, 2010) (**Fig. 1C**) and the profile is attached to the cave wall at the passage junction with a slightly corroded side fissure. The section is horizontally divided into two parts — a longer left segment and shorter right one. The shorter segment shows a different evolutionary history in the upper part; it is partly detached from the longer segment along the crack and has slightly subsided. The boundaries of both segments are expressed by columnar stalagmites at different vertical positions (to the right of the position of the RP profile in **Fig. 1C**) and three principal parts may be distinguished in a vertical profile (Pruner *et al.*, 2003; Zupan Hajna *et al.*, 2008) (**Fig. 1C**). The magnetostratigraphic log obtained was sufficiently correlated with the GPTS of

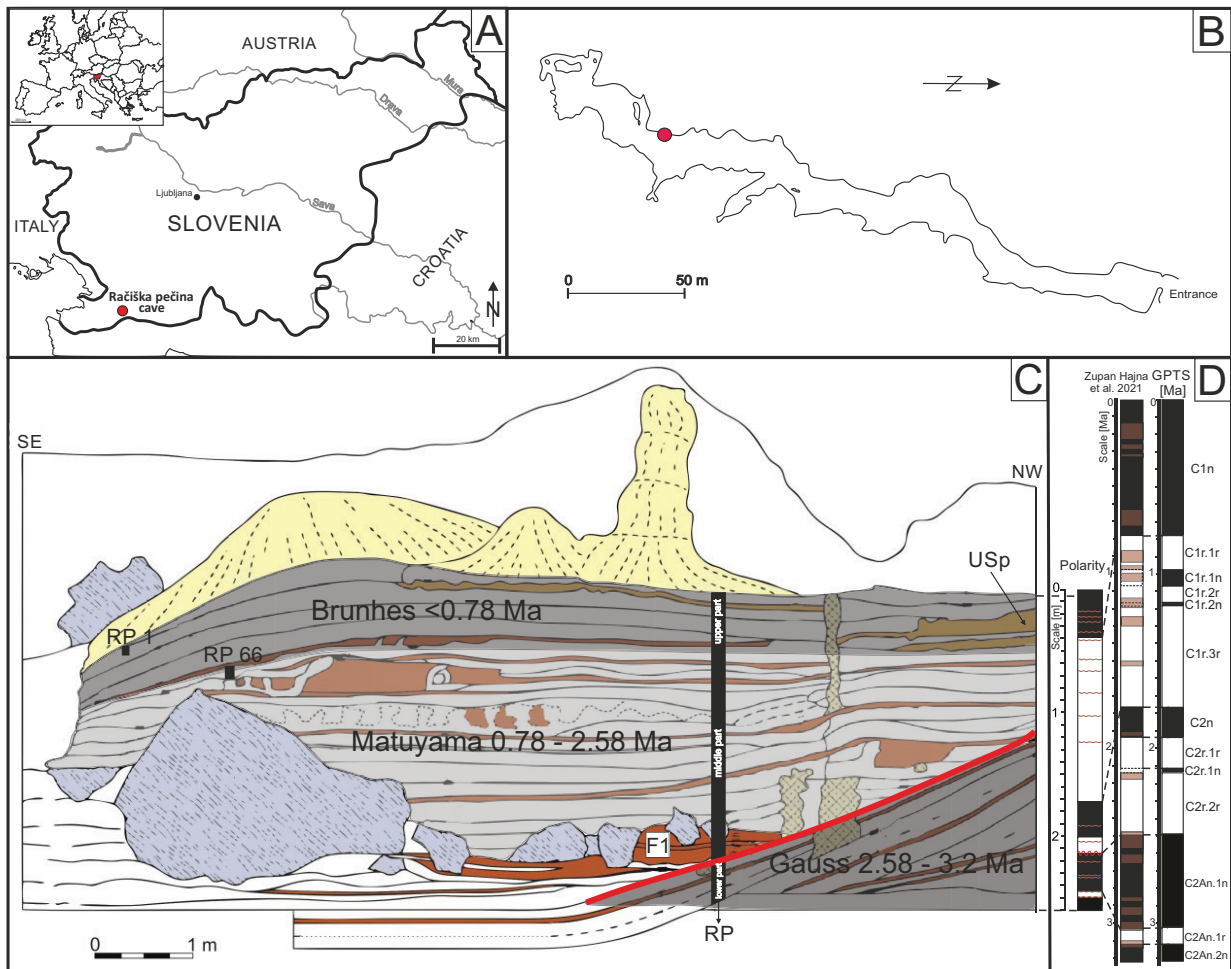


Fig 1. (A) Location of the study site in Slovenia; (B) cave map and profile location (marked with a red circle) (modified from Zupan Hajna *et al.*, 2008); (C) studied profile scheme: grey shading — flowstones; brown shading — clays; diagonal shading (light blue) — collapsed limestone blocks; yellow crosshatching — younger speleothem cover; red line — principal disconformity; F1 — faunal position; USp — position of *Ursus speleus sp* (cave bear) bone fragments; RP — sampling profile for C and O isotope analyses; and (D) magnetostratigraphic log according Pruner *et al.*, (2009) correlated with the GPTS (Cande and Kent, 1995); black — normal polarity, white — reverse polarity, grey — transitional polarity, wavy line — disconformity. GPTS, Geomagnetic polarity time scale.

Cande and Kent (1995) biostratigraphically (Horáček *et al.*, 2007; Moldovan *et al.*, 2011). The past application of multiple different dating methods (see also Zupan Hajna *et al.*, 2008, 2010, 2020, submitted) means that the RP profile contains the best-dated cave sediments in Slovenia. The cave evolution was related to local contact karst characteristics (Mihevc, 2001, 2007); the location of the recent ponors of allogenic streams flowing from the Eocene Flysch towards springs at the Adriatic Sea was confirmed by tracer test (Krivic *et al.*, 1989). The cave was located deep in karst as a part of a larger cave system and the cave functioned at 3.2 Ma ago (Zupan Hajna *et al.*, 2008) as a conduit for underground water flows from the impermeable flysch catchment area to the springs. Before the speleothem dome began to grow, the cave was disconnected from its

hydrological function due to the regional tectonic uplift (Mihevc, 2007), but remained there without the direct ventilation. The cave was later opened to the surface by surface chemical denudation and slope retreat; during this period, cave bears started to enter the cave. The recent phreatic conduits are positioned about 200 m below Račiška pečina and due to an average karst denudation rate of 20–60 m/Ma (Mihevc, 2001) in the area, the cave was opened to the surface in the last 0.5 Ma.

The RP profile can be divided into three lithostratigraphic units namely lower, middle and upper. The lower unit represents three growth stages of a massive vaulted speleothem dome built by brown to reddish-brown massive, highly porous speleothem layers (up to 25 cm thick) with interbedded red muds (1–2 cm thick). The internal

speleothem texture is laminated (sub-millimetre laminae to millimetre-sized bands) and mostly composed of columnar and radial-columnar coarse-grained calcite crystals. There are also several very thin (centimetres in thickness), light-coloured bands of fine-grained (micritic) speleothem beds with a porcelaneous macroscopic appearance. The bottoms of the beds above the muddy intercalations often contain clasts of underlying muds. Fenestrate (vuggy) porosity occurs in places, and part of the porosity is surely intercrystalline among large calcite crystals, while some pores represent the effects of later corrosion. Two unconformities separate individual growth stadia. Broken stalagmites are preserved at the top of the upper (top) two sequences. With respect to the GPTS-matched magnetostratigraphic log, the highest possible age limits of the basal section are found to be from >3.2 Ma (bottom) to ~2.58 Ma (top, i.e., the bottom of the middle profile; Horáček *et al.*, 2007) (**Fig. 1C, D**).

The middle unit of the RP profile predominantly consists of sub-horizontal, laminated to banded, sometimes wavy bedded, partly porous flowstones that are reddish-brown to brownish red in colour, with rimstone dams filled with red and red-brown muds. The internal walls of the rimstones are covered by crystalline corallites. The fill of one rimstone (to the right of sample RP66, **Fig. 1C**) contain oribatid mites, which are forest taxa dated to the Early Pleistocene, specifically to the termination of the Olduvai Subchron (Moldovan *et al.*, 2011). Individual thinner beige beds (centimetres in thickness) are fine-grained and there are several red mud intercalations (1-mm to up to 21-cm-thick). Red muds found to contain mainly quartz along with some muscovite/illite and chlorite, hematite and magnetite, or kaolinite and feldspar, based on X-ray diffractometry. Some muds also contain small iron-rich spherules. Thin calcified siltstones with flowstone fragments and iron-rich spherules occur in places. Near the base of this unit, collapsed blocks from the ceiling cover thicker layers of red muds with faunal remains (F1 in **Fig. 1C**) dated as Early to Middle Pleistocene MN17 (ca. 1.8–2.4 Ma; Horáček *et al.*, 2007). Fauna-containing sediments are underlain by several flowstone layers that unconformably overlay the principal unconformity that terminates the lower section. The bottom of the middle unit is dated to ~2.58 Ma according to magnetostratigraphic and biostratigraphic correlations (Horáček *et al.*, 2007) (**Fig. 1C, D**).

The upper unit of the RP is mostly represented by light-coloured (honey, ochre etc.), thickly bedded, and densely laminated flowstones. Sub-millimetre to millimetre-scale laminae are sub-horizontal, sometimes slightly wavy, or uneven. The internal texture consists of fine columnar to radial-columnar facies with distinct fine laminae, sometimes with distinct porosity (both primary intracrystalline and partly corroded). Basal beds show greater crystal

sizes and higher porosity, and a reddish colour begins to appear. Light-coloured, porcelaneous, thin beds also occur in places. The uppermost flowstone layers have laminae to thin bands enriched in organic carbon (soot), which can be attributed to repeated early human settlements in the cave. Two lenses of brown-yellowish loams interbedded in the right part of the profile contain bone fragments of *Ursus speleus* sp. (cave bear) and clearly indicate a Pleistocene age (**Fig. 1C**). The left segment contains only one such layer, most likely correlating with the upper layer in the right segment. Several old, massive, conical stalagmites, which grow from the top of the middle unit, represent the top of the section. The bottom of the upper part lies at the Brunhes-Matuyama boundary (0.78 Ma; Horáček *et al.*, 2007) (**Fig. 1C, D**). Mud present in between the flowstone layers in all parts of the RP profile resulted from the successive flooding deposition of well-sieved allochthonous sediments from a suspension (Horáček *et al.*, 2007) passing through the fissure system in the epikarst and vadose zones and emptying at the intersection of the narrow side passage with the wide main cave corridor.

3. Regional Climate

Slovenia is influenced by several climate types, reflecting its geographic position. The climate is a mixture of (1) continental climate, which influences the major part of the country; (2) alpine climate, which prevails in the mountains of NW Slovenia; (3) coastal Mediterranean climate, which influences the south-western part of the country. Four major types of air masses influence the weather in Slovenia and they are (1) maritime polar air masses, which originate in the North Atlantic and North Sea; (2) maritime tropical air masses, which predominantly originate in the Azores area; (3) continental tropical air masses originating in northern Africa and Anatolia; and (4) continental polar air masses that originate in Scandinavia, Finland, Russia and on the Pannonian (Carpathian) Plain (Mezga *et al.*, 2014).

The RP has a transitional Mediterranean climate, with a mean annual temperature of ~10.4°C according to long-term observations by the Ilirska Bistrica Meteorological Station at 415 m a.s.l., 14 km NE from the cave (<http://meteo.arso.gov.si/>). The warmest month is July (mean temperature: ~16.5°C), and the coldest month is January (mean temperature: ~-5.4°C). The mean annual precipitation is approximately 1.356 cm, with a maximum in October (~164 mm) and a minimum in February (~80 mm). Observations from the Kozina Weather Station, 20 km northwest of the RP, show that the present mean $\delta^{18}\text{O}$ value of local meteoric water changes from -13.8 ‰ in January to -2.2 ‰ in March (Vreča *et al.*, 2005; Mezga *et al.*, 2014).

4. METHODS

4.1. Sampling

Sampling for paleomagnetic and stable isotope studies was conducted with a very dense spacing (Bosák *et al.*, 2002; Zupan Hajna *et al.*, 2008). The samples of unconsolidated sediments (interbedded muds) used for palaeomagnetic analyses usually had centroid distances of 2–7 cm and were collected using non-magnetic plastic boxes (Natsuhara Giken Co., Ltd., Japan) with a size of 20 × 20 × 20 mm and approximate volume of 6.7 cm³. Speleothem samples were taken from the section by cutting a narrow trench with a powered circular saw (Bosák *et al.*, 2002; Zupan Hajna *et al.*, 2008; Pruner *et al.*, 2009). The continuous slices or columns obtained were then cut into 20 × 20 × 20-mm cubes in the laboratory. All hand specimens were collected *in situ*. Dip directions were measured with a geological compass, and the north direction was drawn on the samples. All data were recorded *in situ* in field drawings and notes.

The samples used for stable isotopic analyses had two sources: (1) plates cut from the original palaeomagnetic samples (columns, slices) in the lower part of the section (i.e. in the domed speleothem below the principal unconformity) and at the top of the section; (2) the originally sampled RP profile above paleomagnetic sample No. RP 71 up to nearly the top of the section (RP line in Fig. 1C). The RP profile was situated at the centre of the sedimentary section which is in its longer left segment. Its position was selected with respect to (1) high-resolution stratification, including the preserved interlamination and interbedding of muds and flowstones pinching out toward both the right and left, and (2) previous magnetostratigraphic results used to cover the entire N-polarised magnetozone interpreted as the Olduvai Subchron (e.g., Horáček *et al.*, 2007).

Flowstone laminae and beds were sampled relative to the orientation of *the in situ* hand specimens. Specimens were collected using a geological hammer and/or chisel, and sometimes taken only by hand. A total of 70 calcite speleothem samples with thicknesses ranging from 0.5–21 cm were obtained; some contained muddy intercalations. Solid samples were separated by laminae to beds of mud that ranged from sub-millimetre up to 15 cm in thickness.

4.2. Stable Carbon and Oxygen Isotope Analyses

Samples collected for $\delta^{13}\text{C}$ and $\delta^{18}\text{O}$ analyses were drilled using a drill (Dremel, USA) bit of diameter of 0.7 mm. All samples were taken along the RP profile with a mean resolution of 5 mm, producing 375 samples. Analyses of the C and O isotope compositions ($\delta^{13}\text{C}$ and $\delta^{18}\text{O}$, respectively) in carbonates were performed using a KIEL IV Carbonate Device coupled to a Delta Plus isotope ratio mass spectrometer (IRMS) using a dual inlet system (Thermo Fisher

Scientific, USA). Sample preparation was carried out automatically.

Approximately 100 μg of calcite was reacted with anhydrous orthophosphoric acid at 70°C for 5 min. The isotopic composition of the released CO_2 was then measured using a Finnigan Delta Plus IRMS (Thermo Fisher Scientific, USA). The results were normalised to three international standards: NBS 19, NBS 18 and IAEA CO 8, and were reported relatively to the Vienna Pee Dee Belemnite (VPDB) international standard. The analytical precision (1σ) was yielded 0.03 ‰ and 0.08 ‰ for $\delta^{13}\text{C}$ and $\delta^{18}\text{O}$, respectively. Reproducibility was assessed by measuring two internal standards after every 12 samples (for $\delta^{13}\text{C}$: ± 0.03 ‰; for $\delta^{18}\text{O}$: ± 0.08 ‰). Analyses were performed in the Stable Isotope Laboratory at the Institute of Geological Sciences, Polish Academy of Sciences in Warsaw.

4.3. U-Series Dating

A series of 0.5 to 1.0 g calcite samples were drilled from samples from the upper part of the RP flowstone (marked as RP66 and RP 1 in Fig. 1C). Only the parts with no macroscopically visible traces of porosity or secondary alteration were selected for dating. Following the thermal decomposition of organic matter, the samples were spiked with a ^{233}U – ^{236}U – ^{229}Th mixture prior to further chemical treatment. The calcite samples were dissolved in nitric acid. Uranium and thorium were separated from the carbonate matrix via chromatography with TRU Resin (Hellstrom, 2006). Standard and blank samples were prepared simultaneously for every series. The mass abundances of ^{233}U , ^{234}U , ^{235}U , ^{236}U , ^{229}Th , ^{230}Th and ^{232}Th were measured using a double-focusing sector field inductively couple plasma–mass spectrometer (ICP–MS) (Element 2, Thermo Finnigan MAT; Thermo Fisher Scientific, USA) at an ICP–MS laboratory in the Institute of Geology, Czech Academy of Sciences in Prague, Czech Republic. Measured results were corrected to account for background and chemical blanks and the final results were reported as isotopic ratios. Uranium-series ages were iteratively calculated from the $^{230}\text{Th}/^{234}\text{U}$ and $^{234}\text{U}/^{238}\text{U}$ activity ratios using the following decay constants (year⁻¹): $\lambda_{238} = (1.55125 \pm 0.0017) \cdot 10^{-10}$ (Jaffey *et al.*, 1971), $\lambda_{234} = (2.826 \pm 0.0056) \cdot 10^{-6}$ (Cheng *et al.*, 2000), $\lambda_{232} = (4.95 \pm 0.035) \cdot 10^{-11}$ (Holden, 1990), and $\lambda_{230} = (9.1577 \pm 0.028) \cdot 10^{-6}$ (Cheng *et al.*, 2000, 2013).

4.4. Reconstructing Speleothem Chronology

The studied RP profile contained several age benchmarks and (Fig. 1C) was not continuous (i.e. calcite layers are bedded by clastic layers). Therefore, it was not possible to estimate one continuous chronology based only on the set of available benchmarks. Many calcite segments do not contain any age benchmarks. The OIS method was used to attempt reconstructing a continuous chronology for

the profile. This method is based on correlating the studied $\delta^{18}\text{O}$ record with a reference $\delta^{18}\text{O}$ curve (Imbrie *et al.*, 1984). The reference curve should meet two basic requirements. First, its age scale must be well defined and second, the reaction of $\delta^{18}\text{O}$ values to climatic changes must be known, and it should be possible to compare it with the studied $\delta^{18}\text{O}$ record.

Here, two records were used as potential reference curves. The first one, the global curve (LR04), is a stack record based on 57 cores with recorded carbonate isotopic variations from foraminiferal tests (Lisiecki and Raymo, 2005). The second curve is the regional Mediterranean (Medi) curve, which is based on stable isotopic records from planktonic foraminifera in the MD84641 core (Wang *et al.*, 2010). Oxygen isotope stratigraphic correlations were performed using Gen-Corr v. 1 software (Pawlak and Hercman, 2016). Three types of benchmarks were implemented in Gen-Corr: (1) ‘fixed’ benchmarks, such as the known age at a specific point in the profile; (2) ‘normal’ benchmarks, such as the age information at a specific point described by a probability distribution, and (3) ‘border’ benchmarks, including age information described by age limits (e.g. younger than 3.2 Ma, etc.). The ages assigned for fixed benchmarks remained constant throughout the correlation procedure, while the ages of non-fixed benchmarks could change according to their probability distributions.

Age estimates for the points between benchmarks were required to meet two conditions: (1) the results must agree with the point stratigraphic position and (2) the ages must be in accordance with the ages of the benchmarks (Pawlak and Hercman, 2016). Here, three paleomagnetic benchmarks were used: (i) the Brunhes–Matuyama boundary, with an age of 780 ka at a depth of 280 mm; (ii) the penultimate benchmark, based on the age of the principal disconformity, which was magnetostratigraphically dated to 2.58 Ma; and (iii) magnetostratigraphic results, assuming that the entire outcropping profile could not be older than ~3.2 Ma (Horáček *et al.*, 2007; Zupan Hajna *et al.*, 2008; Pruner *et al.*, 2009), and one reliable U-series age was used as the age benchmark (sample RP 1). Additionally,

there is another sampled core in this profile, RP66 (Pruner *et al.*, 2009; Hercman *et al.*, submitted), covering Brunhes–Mathuyama reversal and for which a high-resolution age-depth model exists based on paleomagnetic benchmarks and OIS correlations. The location of the RP66 sample in the RP profile can be easily defined via stratigraphic correlation (**Fig. 1**). The calculated borders of the RP66 profile (Hercman *et al.*, submitted) were used as the two additional benchmarks for reconstructing the chronology of the studied RP profile (**Table 1**).

Marine carbonate and speleothem $\delta^{18}\text{O}$ records respond in a similar way to climatic changes (see companion paper for detailed discussion, e.g. Almogi-Labin *et al.*, 2009; Affek *et al.*, 2014). Over long timescales, the global volume of glacial ice impacts the $\delta^{18}\text{O}$ value of ocean surface waters (Dansgaard, 1964). In low-temperature conditions, the ocean surface water becomes depleted in ^{16}O since evaporation process prefers this isotope. The development of ice sheets cover during glacial periods leads to tapping enriched in ^{16}O water. Therefore, over long timescales, the global volume of glacial ice impacts the $\delta^{18}\text{O}$ value of ocean surface waters (Dansgaard, 1964). The changes of speleothem carbonate $\delta^{18}\text{O}$ value are more complex, they depend on $\delta^{18}\text{O}$ of dripping water, which is driven by several factors such as source effect, the temperature effect at evaporation and atmospheric precipitation sites. Additionally, the local factors like evaporation at precipitation site or during the water percolation play an important role. All these factors can strengthen each other or eliminate their effects. At the coastal site, the source effect remains strong. Farther in the continental interior the source effect is more modified by continental effects and the temperature effect. Evolving from glacial to interglacial conditions the source effect would shift the speleothem $\delta^{18}\text{O}$ value to the more negative direction, while the ambient air temperature effect would result in higher speleothem $\delta^{18}\text{O}$ value. At Mediterranean coastal sites, the $\delta^{18}\text{O}$ values of speleothem are determined by the temperature during the speleothem formation, the source effect and amount of precipitation water. In summary, during warm periods the deposited speleothem calcite can be enriched in $\delta^{18}\text{O}$. Therefore, marine data are

Table 1. Detailed data of benchmarks used for OIS.

No.	Age (Ma)	Age uncertainty	Depth in RP profile (mm)	Depth uncertainty (mm)	$\delta^{18}\text{O}$ [‰]	$\delta^{13}\text{C}$ [‰]	Type of benchmark
1	0.12	0.02	65	2.5	-4.90	-6.84	U-series age
2	0.495	0.015	210	2.5	-5.32	-9.20	Age at model*
3	0.78	0.0117	280	2.5	-5.45	-9.22	Paleomagnetic
4	0.80	0.02	295	2.5	-5.39	-9.72	Age at model*
5	2.58	0.0387	1572.5	2.5	–	–	Paleomagnetic
6	3.2	0.048	1860	2.5	-5.28	-7.75	Paleomagnetic

OIS, Oxygen isotope stratigraphy.

*Ages obtained from borders of the RP66 flowstone (on **Fig. 1**) made by Hercman *et al.*, submitted.

presented on the inverted scale for correlation purposes. However, the amplitude of changes and mean values of $\delta^{18}\text{O}$ for speleothems and marine records differ. Therefore, the normalisation of $\delta^{18}\text{O}$ data must precede correlation. The normalisation eliminates the effect of amplitudes and shifts in absolute value. In this study, both reference and studied records were normalised by scaling to 0–1 range. After that, the records were correlated using modified Gen-Corr software (Pawlak and Hercman, 2016), which seeks to identify the highest similarly (optimal correlation) between two records using a genetic algorithm. Additionally, Gen-Corr allows the use of *a priori* age information during the correlation procedure, which allows the use of reliable benchmarks. The Gen-Corr seeks the optimal position between correlated records using similarity indicator. The used similar indicator is the mean distance between the correlated records.

5. Results

5.1. Stable Carbon and Oxygen Isotope Compositions

Analyses of 375 samples resulted in the construction of $\delta^{13}\text{C}$ and $\delta^{18}\text{O}$ records (Fig. 2). These records revealed that isotopic compositions changed significantly during the deposition of the RP profile. The $\delta^{13}\text{C}$ values varied from -3.4‰ to -11.2‰ , while the $\delta^{18}\text{O}$ values varied between -4.2‰ and -7.1‰ . The most conspicuous changes were observed near the main discontinuity (red solid line in Fig. 2), before which the $\delta^{13}\text{C}$ values had amplitudes of $\sim 3\text{‰}$ and after were $\sim 7\text{‰}$. For the $\delta^{18}\text{O}$ values, before the main

discontinuity, the amplitudes were $\sim 0.5\text{‰}$ and after, they were $\sim 2\text{‰}$. Additionally, at a depth of $\sim 900\text{ mm}$, there was a visible change in the frequencies of the $\delta^{13}\text{C}$ and $\delta^{18}\text{O}$ records. The minimum C isotope values were found at depths of $340\text{--}200\text{ mm}$; there was also a decline in the O isotope values over the same depth range.

5.2. U-Series Results

The age of the lower part of the studied flowstone was beyond the U-series limit, unlike the upper part of the RP profile. Despite very high contamination by clays, iron oxides and hydroxides, and a relatively low U content ($\sim 0.1\text{ ppm}$), it was possible to date only two samples collected in the upper part of the RP flowstone (Table 2; Fig. 1C). The RP 1 sample corresponded to the profile sample at a depth of 65 mm , for which the age was $120 \pm 20\text{ ka}$. The age uncertainty of RP66 is so large that it prevents from dating, so this sample cannot be dated by U-Th series dating.

5.3. Chronology Estimates Based on OIS

Further, to establish the OIS chronology, the RP profile (Fig. 1C) was divided into two segments, separated by the principal discontinuity (red line in Fig. 1C). Initially, both parts of the RP profile were correlated with the Medi and LR04 curves. The Gen-Corr seeks the optimal position between correlated records using similarity indicator. The similar indicator used (as above) is the mean distance between the correlated records. Both sections showed different similarity indicators with specific reference curves (Fig. 3). The OIS results showed that the $\delta^{18}\text{O}$ record from the lower segment (below the unconformity) of the profile

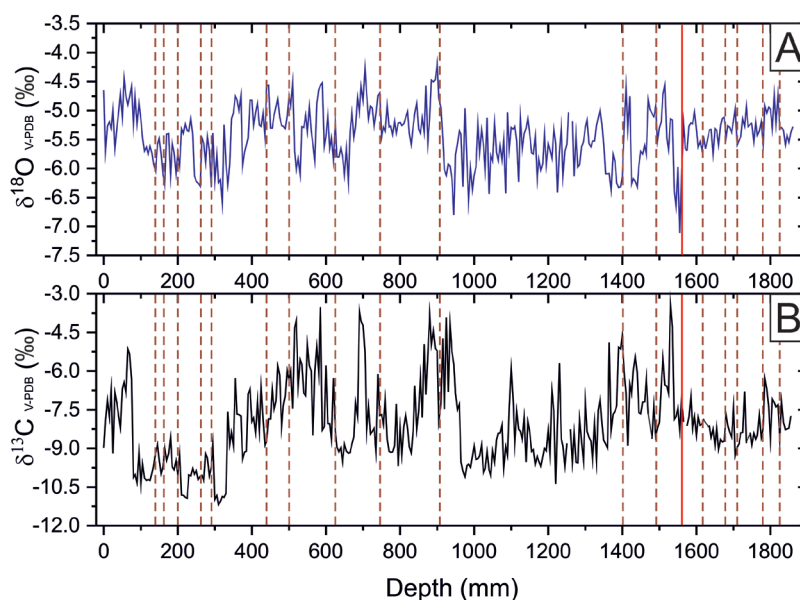


Fig. 2. Stable oxygen (A) and carbon (B) isotope compositions in the RP profile. Vertical red lines — principal discontinuity; vertical, dotted, and brown lines — main clay layers.

Table 2. Results of U-series dating of the RP profile.

Lab. no.	Sample	U cont. (ppm)	$^{234}\text{U}/^{238}\text{U}$ AR	$^{230}\text{Th}/^{234}\text{U}$ AR	$^{230}\text{Th}/^{232}\text{Th}$ AR	Age (ka)	*Corrected age (ka)
1537	RP 1	0.1236 ± 0.0061	1.117 ± 0.067	0.698 ± 0.045	14 ± 3	126 ⁺¹⁴ ₋₁₃	120 ± 20
1538	RP66	0.1239 ± 0.0049	1.239 ± 0.059	1.068 ± 0.051	1.184 ± 0.052	>450	(440 ^{+inf} ₋₁₃₀)

The reported errors are 2s.

Calculations use the decay constant of Jaffey *et al.*, 1971 (^{238}U), Cheng *et al.*, 2013 (^{234}U and ^{230}Th) and Holden, 1990 (^{232}Th). Ages do not include uncertainties associated with decay constants. Reported errors are equal to 2s.

AR, Activity ratio.

*Age adjusted for detrital contamination, indicated by the presence of ^{232}Th , using the typical silicate activity ratio $^{230}\text{Th}/^{232}\text{Th} = 0.83 \pm 0.42$, derived from the following activity ratios: $^{232}\text{Th}/^{238}\text{U} = 1.21 \pm 0.6$, $^{230}\text{Th}/^{238}\text{U} = 1.0 \pm 0.1$, and $^{234}\text{U}/^{238}\text{U} = 1.0 \pm 0.1$ (e.g., Cruz *et al.*, 2005).

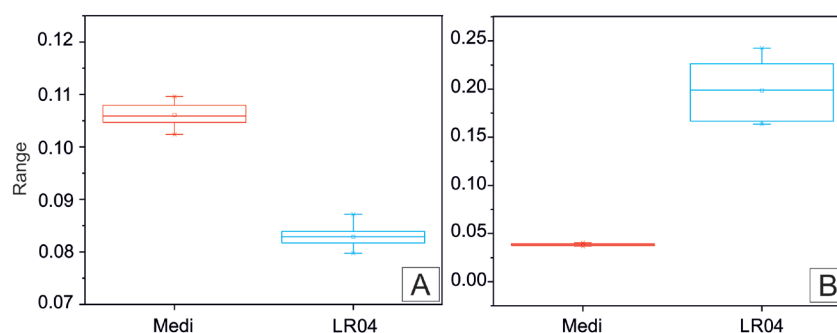


Fig 3. Comparison of similarity indicators in the Medi and LR04 records to the RP oxygen isotope composition (calculation in Gen-Corr by Pawlak and Hercman, 2016); **(A)** boxplots for the upper part of the RP profile and **(B)** boxplots for the lower part of the RP profile; the vertical axis represents the 2s uncertainty of the similarity indicator.

matched the $\delta^{18}\text{O}$ reference curve (Medi curve) from ~3.20 to 2.58 Ma, which is much better than that of LR04. Meanwhile, the upper segment (above the unconformity) fit the $\delta^{18}\text{O}$ global reference curve (LR04) from ~2.48 Ma to ~80 ka.

Age–depth models for RP profile segments were constructed independently from 80 correlations for each pair of curves (**Fig. 4**). During correlation, the number of depositional breaks was identified (grey sections in **Fig. 4**). The lower segment was divided into five parts, and the upper segment was divided into 15 parts.

The hiatuses designed by the correlation process agreed with the locations of clay intercalations observed macroscopically in both parts of the profile. The longest hiatus, at the time of the principal disconformity, was ~100 ka long (from ~2.58 to ~2.48 Ma); the longest hiatus in the lower part of the profile was ~60 ka long (from ~2.89 to ~2.95 Ma) and the shortest hiatus was ~30 ka long (from ~2.75 to ~2.78 Ma). In the upper part of the RP profile, the longest break lasted ~100 ka (from ~650 to ~750 ka) and the shortest break was ~25 ka long (from ~310 to ~335 ka).

6. Discussion

6.1. Reliability of the Chronology

An OIS age–depth model was constructed for the RP profile based on 80 iterations. Due to many numbers of

correlations, it was possible to establish that the age range of the profile was from ~3.2 Ma to 0.08 Ma, which includes marine isotope stages (MIS's) Km3 to 5 (**Fig. 5**). The uncertainty of the model was 2 σ bands. The similarity indicator for the lower segment was 0.082 and for the upper segment, it was 0.19 (**Fig. 3**). Therefore, the reliability of the lower part appears to be higher. However, the similarities of the segments to the reference curves were not uniform over time. In the case of the older profile segment, the segments were most similar in the following age ranges: from 3.1 Ma to 3.40 Ma and from 3.0 Ma to 2.95 Ma. Meanwhile, in the younger part, the sections in the following age ranges showed the greatest similarities to the reference curve (LR04): from 2.18 Ma to 1.50 Ma, from 1.25 Ma to 1.125 Ma and from 875 ka to 750 ka. The reliability of the correlation was higher in segments when the similarity indicator was lower (Pawlak and Herman, 2016).

6.2. Factors Shaping the Reference Curves

The LR04 curve is based on 57 deep-sea cores, which record isotopic variations in the carbonate tests of foraminifera (Lisiecki and Raymo, 2005). The $\delta^{18}\text{O}$ of foraminiferal tests is a function of the temperature and $\delta^{18}\text{O}$ of the water in which they form, and the $\delta^{18}\text{O}$ of seawater is a function of global ice volume and ocean salinity (Lisiecki and Raymo, 2005). The water in the deep ocean is more uniform in temperature and salinity than are surface

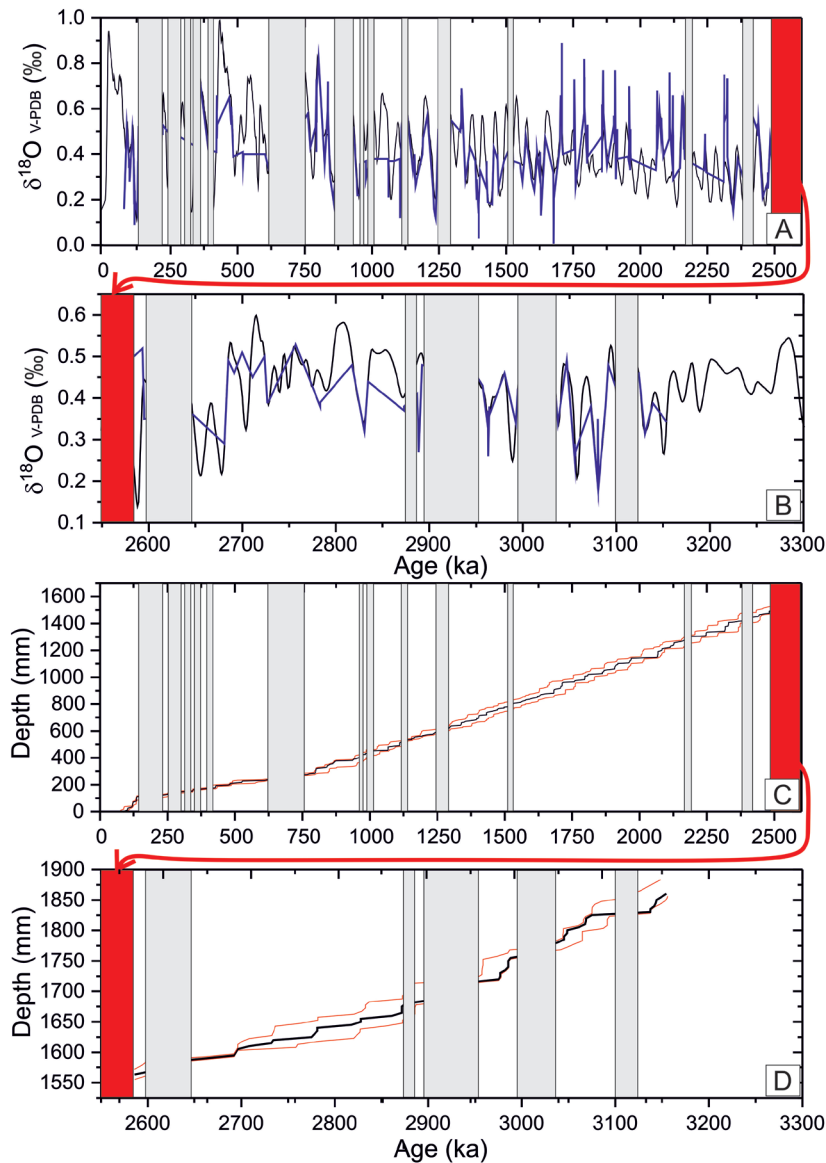


Fig 4. Correlation results of the RP oxygen isotope record with the LR04 and Medi records. All data presented were normalised and the marine $d^{18}\text{O}$ data were inverted. **(A)** RP curve (blue line) for the upper segment of the profile correlated with the LR04 curve (black line); **(B)** RP curve (blue line) for the lower segment of the profile correlated with the Medi curve (black line); **(C)** age-depth model for the upper segment of the profile; and **(D)** age-depth model for the lower segment of the profile; red lines — confidence intervals; grey boxes — hiatuses; red boxes — principal disconformity.

waters. Therefore, the tests of benthic foraminifera reflect global climate change in a better manner (Lisiecki and Raymo, 2005). In contrast, the Medi curve is represented by the stable isotopic records of the planktonic foraminifer *Globigerinoides ruber* from core MD84641 (Wang *et al.*, 2010). This species lives near the sea surface, and so they are more sensitive to changes in temperature and salinity. Therefore, they better reflect more frequent and smaller changes in the temperature, volume and salinity of seawater (Wang *et al.*, 2010). Moreover, the Mediterranean Sea is well separated from the Atlantic Ocean, and therefore,

its isotopic composition is more dependent on local factors than on global ones.

Speleothem $\delta^{18}\text{O}$ values usually reflect the $\delta^{18}\text{O}$ of moisture, precipitation, and the temperature difference between precipitation site and source region. The isotopic compositions of moisture and precipitation depend on the isotopic composition of their source (s) and the way they are transported (Darling, 2004; Lachniet, 2006). Therefore, speleothem records can be correlated with marine foraminifera records if the source effect is strong enough or if the speleothem record reflects the global changes of temperature.

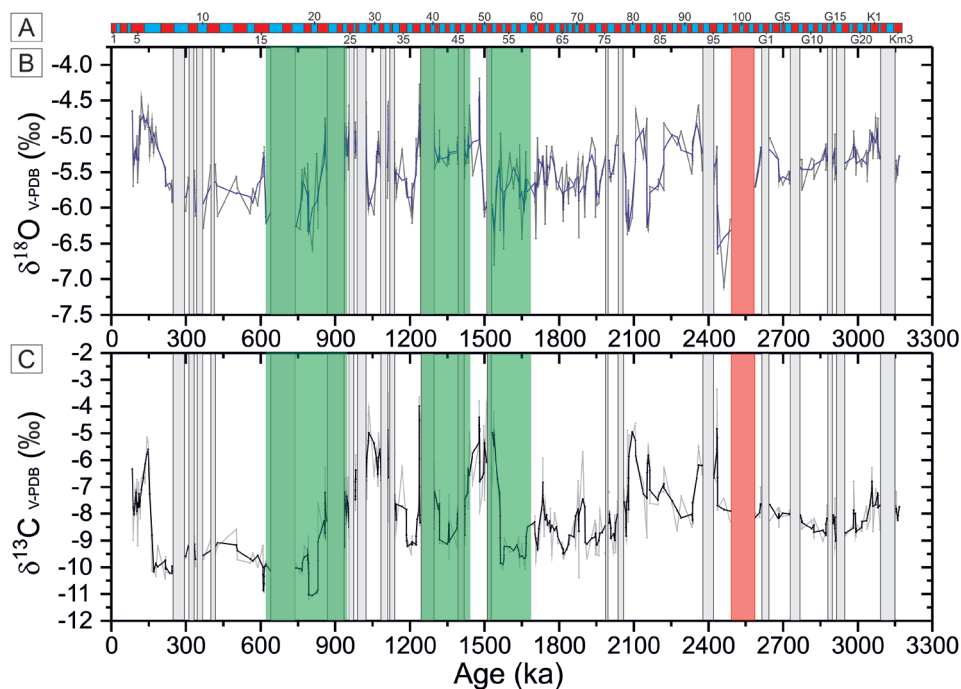


Fig 5. The final set of stable carbon and oxygen isotope records of the RP profile; (A) MIS scale (warm — red; cold — blue) (Lisiecki and Raymo, 2005); (B) stable oxygen isotope record (smoothed data — blue; raw data — grey); and (C) stable carbon isotope record (smoothed data — black; raw data — grey); grey boxes — hiatuses; red box — principal disconformity; green boxes — episodes where the R^2 value is significantly greater, $R^2 = 0.4538$, $R^2 = 0.4944$, and $R^2 = 0.6065$. MIS, Marine isotope stage.

6.3. Local Factors Influencing the RP Record

Speleothems from the Middle East record $\delta^{18}\text{O}$ changes like the same patterns as those of the Mediterranean cores (i.e. source effect) (Bar-Matthews *et al.*, 1999; Orland *et al.*, 2012).

At the site of precipitation, isotopic compositions are modified by local conditions, such as the ambient air temperature and amount of rainfall (Róžański *et al.*, 1993). The thermal gradient for calcite crystallisation ($\delta^{18}\text{O}_{\text{Oct/dt}}$) varies from -0.18‰ to -0.23‰ , while that for the $\delta^{18}\text{O}$ of precipitated water ($\delta^{18}\text{O}_{\text{Op/dt}}$) ranges from $+0.17\text{‰}$ to $+0.9\text{‰}$ (Róžański *et al.*, 1993; Lachniet, 2006). Speleothem $\delta^{18}\text{O}$ responses to temperature are strongly site-dependent (Williams *et al.*, 1999; Mangini *et al.*, 2005). Observations from the weather station in Kozina, Slovenia, 20 km northwest of the cave, show that the present $\delta^{18}\text{O}$ value of local meteoric water ranges from -13.8‰ in January to -2.2‰ in March (Vreča *et al.*, 2005; Mezga *et al.*, 2014). However, March is not the warmest month in a region. Therefore, the fact that the March rainwater has the maximum $\delta^{18}\text{O}$ value shows that not only the temperature but also other factors such as the source of moisture and its transportation that play important roles in shaping the $\delta^{18}\text{O}$ value of rainwater in the studied region. Moreover, this seasonal difference shows how strongly the mean annual isotopic composition depends on the amount of rainfall in particular seasons.

In winter and autumn, the influence of Atlantic air masses prevails over the study area and is associated with an increased amount of rainfall during this time. In contrast, in spring and summer, influences from the Mediterranean Sea dominate when rainfall is lower throughout the year (Milošević *et al.*, 2017). The source of rainfall also varies by season and is related to seasonal changes in the circulation of air masses. Past studies have shown that, in January, sources from the Atlantic Ocean prevail, and for the rest of the year, rainfall from the Mediterranean region dominates (Róžański *et al.*, 1993; Vreča *et al.*, 2005; Mezga *et al.*, 2014). Presently, the main source of moisture for the region is the southern-most Mediterranean, and a small amount of moisture is transported from the Atlantic (Vreča *et al.*, 2005). The water from the Mediterranean source is enriched in $\delta^{18}\text{O}$ in comparison to the Atlantic-derived moisture due to stronger evaporation effect in the Mediterranean basin. The processes that occur in karst environments can shape the $\delta^{18}\text{O}$ of speleothems. Generally, in paleoclimatic interpretations, equilibrium isotopic fractionation is preferred because such fractionation only depends on temperature (Mangini *et al.*, 2005). Progressive enrichments of $\delta^{13}\text{C}$ and $\delta^{18}\text{O}$, along with the profile and/or a positive correlation of the two isotope compositions, indicate that fractionation occurred under kinetic conditions (Mickler *et al.*, 2015). Additionally, another way to determine whether a

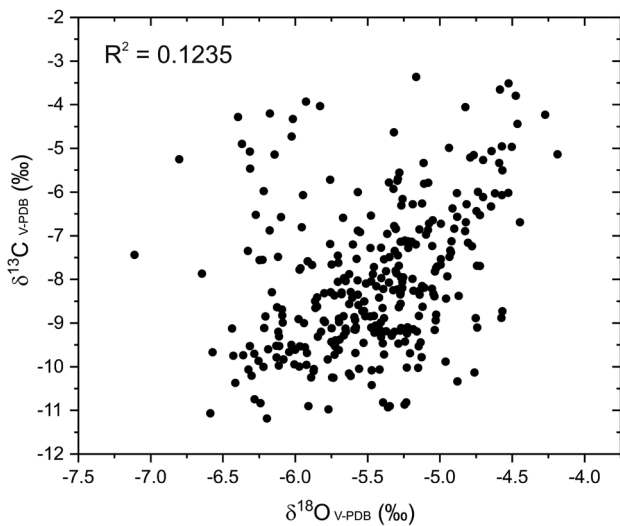


Fig 6. Correlation of $\delta^{13}\text{C}$ and $\delta^{18}\text{O}$ values from the entire RP profile ($p < 0.05$).

speleothem was formed at isotopic equilibrium involves samples taken along the growth axis lacking a positive correlation in $\delta^{13}\text{C}$ and $\delta^{18}\text{O}$ values (Goede *et al.*, 1986; Goede, 1994; Desmarchelier *et al.*, 2000; Mickler *et al.*, 2015). In the case of the whole RP flowstone, the compilation of $\delta^{13}\text{C}$ and $\delta^{18}\text{O}$ values showed no positive correlation, with $R^2 = 0.1235$ (**Fig. 6**). However, there were three episodes in the profile where the R^2 value ($p < 0.05$) was significantly greater: 632–954 ka, $R^2 = 0.4538$; 1.246–1.456 Ma, $R^2 = 0.4944$; 1.525–1.676 Ma, $R^2 = 0.6065$ (**Fig. 5B, C**). The correlation of $\delta^{13}\text{C}$ with $\delta^{18}\text{O}$ may be caused by the effect of kinetic fractionation, but in some cases, it may be caused by climatic conditions (Dorale and Liu, 2009). The $\delta^{13}\text{C}$ proxy reflects the level of soil development and the residence time of water in the karstic landscape. Both factors depend on the volume of precipitation (e.g., Lachniet, 2009).

6.4. Similarities of the RP Record to the Medi and LR04 Reference Curves

The marine data used by the authors are presented on an opposite scale to the speleothem data (see Section 4.4.). The RP profile is divided by the principal disconformity. The older part of the record can be better correlated with the Medi reference curve, while the younger part is more similar to the LR04 reference curve. This main difference between these correlations may reflect the long-term changes in the main source of vapour and atmospheric circulation in the region. However, the similarity of the segments to the chosen reference curves is not uniform (see Section 6.1). The affinity for the Medi reference curve to the RP record may be caused by the source effect. Rainfall over the cave area inherits the isotope signature of the northern

Mediterranean Sea or the eastern Atlantic Ocean. The resulting $\delta^{18}\text{O}$ recorded in speleothems is strongly influenced by marine reservoirs contributing vapour to rain formation (Kolodny *et al.*, 2005; Burstyn *et al.*, 2019). This also means that, over the age ranges in which the RP record is most similar to the reference curves, these sources were of the greatest importance in shaping the isotopic composition of the speleothems. Moreover, one should also consider why the rest of the record from the RP does not match the reference curves as well as the aforementioned segments of the profile. This discrepancy may be due to local factors affecting the isotopic composition, such as differences in local water circulation, mean annual air temperature and the amount of precipitation.

In addition, the youngest part of the RP record has been compared with speleothem records from other caves in the Mediterranean region: the Soreq cave and Peqiin cave in Israel (Bar-Matthews *et al.*, 2003), Antro del Corchia cave located in Alpi Apuane karst in Italy (Drysdale *et al.*, 2005) and Pentadactylos cave on Cyprus (Nehme *et al.*, 2020). The noticeable similarities between the shapes of the RP $\delta^{18}\text{O}$ and $\delta^{13}\text{C}$ records to the Soreq, Peqiin, Antro del Corchia and Pentadactylos records during MIS 5e, which shows the climatic changes across the entire Mediterranean during the last interglacial period. In the $\delta^{18}\text{O}$ curve, there is a noticeable difference in absolute values ($\sim 0.2\text{‰}$), which may be attributable to the differences in the locations of the caves (i.e. the continental effect). Unfortunately, it is not possible to obtain a detailed correlation due to large differences in their resolutions, since one point represents the average time resolution of ~ 0.1 ka in the two Israeli speleothem records while representing ~ 1 ka in the earliest part of the RP record.

7. Conclusions

The RP profile represents a unique data archive, especially for the length of record (approximately the last 3.2 Ma), as well as the uniqueness of the Mediterranean region. The results of this study supplement existing paleoclimate knowledge, as these types of profiles enable us to obtain high-resolution isotope records. Considering their long growth period, especially at the Pliocene–Quaternary boundary, it is truly an important source of climatological information.

At the time of correlation, 19 hiatuses were detected, which corresponded to clay layers present throughout the profile. The RP profile was deposited from ~ 3.2 Ma to ~ 0.08 Ma (MIS Km3 to MIS 5) and was divided into two segments separated by the principal disconformity. The lower segment correlated better with the regional curve, which suggests a greater influence of regional and local

factors at the time of deposition in the cave area. The upper segment correlated better with the global LR04 curve, which may indicate a stronger influence of global changes at that time. Therefore, Slovenian caves may serve as vital sources of climatological information for much older periods and provide excellent materials for more detailed paleoclimate studies in the future.

Nevertheless, for a more accurate reconstruction of paleoclimate, a multi-proxy approach is necessary. However, the application of OIS, combined with magnetostratigraphy and U-Th data, enabled us to establish a more detailed chronology for the RP profile.

Acknowledgments

This work was supported by the Institute of Geological Sciences PAS as an internal project 'OIS', the bilateral mobility co-operations MOBILITY PAN-17-22 between Czech Academy of Sciences and Polish Academy of Sciences, and MOBILITY SAZU-16-03 and SAZU-19-01 between Czech Academy of Sciences and Slovenian

Academy of Sciences and Arts. Sampling, paleomagnetic and paleontological analyses, processing and evaluation were carried out within the KONTAKT program of the Ministry of Education, Youth and Sports of the Czech Republic and Slovenian Ministry of Science and Technology Nos. 28-2003-04, 13-2005-06, and MEB 090619, Grants of the Grant Agency of the Academy of Sciences of the Czech Republic Nos. IAA3013201 and IAA30013001, the Programs of Advancements in Scientific Research in Key Directions of the Academy of Sciences of the Czech Republic (AS CR) No. K3046108, Research Plans of the Institute of Geology AS CR Nos. CEZ A09/98 Z3-013-912 and AV0Z30130516, and the Plan of Institutional financing of the Institute of Geology of the Czech Academy of Sciences No. RVO 67985831. Research activities in Slovenia were covered by research programs of the Ministry of Science of Slovenia and Slovenian Research Agency Nos. P6-0119-0618 and P0-0119, and projects Nos. J6-3035-0618-01 and J6-6345-0618-04. Studies in Slovenia were funded by the Slovenian Research Agency [research core funding No. P6-0119].

REFERENCES

- Affek HP, Matthews A, Ayalon A, Bar-Matthews M, Burstyn Y, Zaarur S and Zillberman T, 2014. Accounting for kinetic isotope effects in Soreq Cave (Israel) speleothems. *Geochimica et Cosmochimica Acta* 143: 303–318, DOI: [10.1016/j.gca.2014.08.008](https://doi.org/10.1016/j.gca.2014.08.008).
- Almogi-Labin A, Bar-Matthews M, Shriki D, Kolosovsky E, Paterne M, Schilman B, Ayalon A, Aizenshtat Z, Matthews A, 2009. Climatic variability during the last 90 ka of the southern and northern Levantine Basin as evident from marine records and speleothems. *Quaternary Science Reviews* 28(25–26): 2882–2896, DOI: [10.1016/j.quascirev.2009.07.017](https://doi.org/10.1016/j.quascirev.2009.07.017).
- Ayalon A, Bar-Matthews M, Kaufman A, 2002. Climatic conditions during marine oxygen isotope stage 6 in the eastern Mediterranean region from the isotopic composition of speleothems of Soreq Cave, Israel. *Geology* 30(4): 303–306, DOI: [10.1130/0091-7613\(2002\)030<0303:CCDMOI>2.0.CO;2](https://doi.org/10.1130/0091-7613(2002)030<0303:CCDMOI>2.0.CO;2).
- Baker A, Wilson R, Fairchild IJ, Franke J, Spötl C, Matthey D, Trouet V and Fuller L, 2011. High resolution $\delta^{18}\text{O}$ and $\delta^{13}\text{C}$ records from an annually laminated Scottish stalagmite and relationship with last millennium climate. *Global and Planetary Change* 79(3–4): 303–311, DOI: [10.1016/j.gloplacha.2010.12.007](https://doi.org/10.1016/j.gloplacha.2010.12.007).
- Bar-Matthews M, Ayalon A, Gilmour M, Matthews A and Hawkesworth CJ, 2003. Sea–land oxygen isotopic relationships from planktonic foraminifera and speleothems in the Eastern Mediterranean region and their implication for palaeorainfall during interglacial intervals. *Geochimica et Cosmochimica Acta* 67(17): 3181–3199, DOI: [10.1016/S0016-7037\(02\)01031-1](https://doi.org/10.1016/S0016-7037(02)01031-1).
- Bar-Matthews M, Ayalon A, Kaufman A and Wasserburg GJ, 1999. The Eastern Mediterranean paleoclimate as a reflection of regional events: Soreq cave, Israel. *Earth and Planetary Science Letters* 166(1–2): 85–95, DOI: [10.1016/S0012-821X\(98\)00275-1](https://doi.org/10.1016/S0012-821X(98)00275-1).
- Bosák P, Hercman H, Mihevc A and Pruner P, 2002. High resolution magnetostratigraphy of speleothems from Snežna Jama, Kamniške-Savinja Alps, Slovenia. *Acta carsologica* 31(3): 15–32. DOI: [10.3986/ac.v31i3.377/](https://doi.org/10.3986/ac.v31i3.377/).
- Bosák P, Pruner P and Kadlec J, 2003. Magnetostratigraphy of cave sediments: Application and limits. *Studia Geophysica et Geodaetica* 47(2): 301–330. DOI: [10.1023/A:1023723708430](https://doi.org/10.1023/A:1023723708430).
- Bosák P, Pruner P, Mihevc A and Zupan Hajna N, 2000. Magnetostratigraphy and unconformities in cave sediments: Case study from the Classical Karst, SW Slovenia. *Geologos* 5: 13–30.
- Bosák P, Pruner P, Mihevc A, Zupan Hajna N, Horáček J, Kadlec J, Man O and Schnabl P, 2004. Račiška pečina. 12th International Karstological School, Classical Karst – Dating of Cave Sediments, Postojna. Guide booklet for the excursions and abstracts of presentations: 23–27, Postojna.
- Burstyn Y, Martrat B, Lopez JF, Iriarte E, Jacobson MJ, Lone MA and Deininger M, 2019. Speleothems from the Middle East: An example of water limited environments in the SISAL Database. *Quaternary Review* 2(2): 16, DOI: [10.3390/quat2020016](https://doi.org/10.3390/quat2020016).
- Cande SC and Kent DV, 1995. Revised calibration of the geomagnetic polarity timescale for the Late Cretaceous and Cenozoic.

- Journal of Geophysical Research* 100(B4): 6093–6095, DOI: [10.1029/94JB03098](https://doi.org/10.1029/94JB03098).
- Cheng H, Edwards RL, Hoff J, Gallup CD, Richards DA and Asmerom Y, 2000. The half-lives of U-234 and Th-230. *Chemical Geology* 169: 17–33, DOI: [10.1016/S0009-2541\(99\)00157-6](https://doi.org/10.1016/S0009-2541(99)00157-6).
- Cheng H, Edwards RL, Shen CC, Polyak VJ, Asmerom Y, Woodhead J, Hellstrom J, Wang Y, Kong X, Spötl C, Wang X and Alexander CE, 2013. Improvements in 230Th dating, 230Th and 234U half-life values, and U–Th isotopic measurements by multi-collector inductively coupled plasma mass spectrometry. *Earth and Planetary Science Letters* 371–372: 82–91, DOI: [10.1016/j.epsl.2013.04.006](https://doi.org/10.1016/j.epsl.2013.04.006).
- Cheng H, Lawrence Edwards LR, Sinha A, Spötl C, Yi L, Chen S, Kelly M, Kathayat G, Wang X, Li X, Kong X, Wang Y, Ning Y and Zhang H, 2016. The Asian monsoon over the past 640,000 years and ice age terminations. *Nature* 534: 640–646, DOI: [10.1038/nature18591](https://doi.org/10.1038/nature18591).
- Cruz FW, Burns SJ, Karmann I, Sharp WD, Vuille M, Cardoso AO, Ferrari JA, Dias PLS and Viana O Jr, 2005. Insolation-driven changes in atmospheric circulation over the past 116,000 years in subtropical Brazil. *Nature* 434: 63–66.
- Dansgaard W, 1964. Stable isotopes in precipitation. *Tellus* 16(4): 436–468, DOI: [10.1111/j.2153-3490.1964.tb00181.x](https://doi.org/10.1111/j.2153-3490.1964.tb00181.x).
- Darling WG, 2004. Hydrological factors in the interpretation of stable isotopic proxy data present and past: A European perspective. *Quaternary Science Reviews* 23: 743–770, DOI: [10.1016/j.quascirev.2003.06.016](https://doi.org/10.1016/j.quascirev.2003.06.016).
- Demeny A, Kern Z, Czuppon G, Németh A, Leél-Össy S, Siklósy Z, Lin K, Hu HM, Shen CC, Vennemann TW and Haszpra L, 2017. Stable Isotope Compositions of Speleothems from the last interglacial E spatial patterns of climate fluctuations in Europe. *Quaternary Science Reviews* 161: 68–80, DOI: [10.1016/j.quascirev.2017.02.012](https://doi.org/10.1016/j.quascirev.2017.02.012).
- Desmarchelier JM, Goede A, Ayliffe LK, McCulloch MT and Morarty K, 2000. Stable isotope record and its palaeoenvironmental interpretation for a late Middle Pleistocene speleothem from Victoria Fossil Cave, Naracoorte, South Australia. *Quaternary Science Reviews* 19: 763–774, DOI: [10.1016/S0277-3791\(99\)00037-2](https://doi.org/10.1016/S0277-3791(99)00037-2).
- Dorale JA and Liu Z, 2009. Limitations of Hendy test criteria in judging the paleoclimatic suitability of speleothems and the need for replication. *Journal of Cave and Karst Studies the National Speleological Society Bulletin* 71(1): 73–80.
- Drysdale R, Zanchetta G, Hellstrom JC, Fallick AE and Zhao J, 2005. Stalagmite evidence for the onset of the last interglacial in southern Europe at 129 ± 1 ka. *Geophysical Research Letters* 32: 1–4, DOI: [10.1029/2005GL024658](https://doi.org/10.1029/2005GL024658).
- Fairchild IJ and Baker A, 2012. *Speleothem Science: From Process to Past Environments*. John Wiley and Sons, DOI: [10.1002/9781444361094.app1](https://doi.org/10.1002/9781444361094.app1).
- Fohlmeister J, Voarintsoac NRG, Lechleitner AF, Boyd M, Brandstätter S, Jacobsong MJ and Osterh JL, 2020. Main controls on the stable carbon isotope composition of speleothems. *Geochimica et Cosmochimica Acta* 279: 67–68, DOI: [10.1016/j.gca.2020.03.042](https://doi.org/10.1016/j.gca.2020.03.042).
- Goede A, 1994. Continuous early last glacial palaeoenvironmental record from a Tasmanian speleothem based on stable isotope and minor element variations. *Quaternary Science Reviews* 13: 283–291, DOI: [10.1016/0277-3791\(94\)90031-0](https://doi.org/10.1016/0277-3791(94)90031-0).
- Goede A, Green DC and Harmon RS, 1986. Late Pleistocene palaeotemperature record from a Tasmanian speleothem: Australian. *Journal of Earth Sciences* 33: 333–342.
- Gradstein FM, Ogg JG, Schmitz MD and Ogg GM, 2012. *The Geologic Time Scale 2012*. Elsevier, DOI: [10.1016/C2011-1-08249-8](https://doi.org/10.1016/C2011-1-08249-8).
- Hellstrom J, 2006. U–Th dating of speleothems with high initial 230Th using stratigraphical constraint. *Quaternary Geochronology* 1(4): 289–295, DOI: [10.1016/j.quageo.2007.01.004](https://doi.org/10.1016/j.quageo.2007.01.004).
- Hendy CH, 1971. The isotopic geochemistry of speleothems – I. the calculation of the effects of different modes of formation on the isotopic composition of speleothems and their applicability as palaeoclimatic indicators. *Geochimica et Cosmochimica Acta* 35: 801–824, DOI: [10.1016/0016-7037\(71\)90127-X](https://doi.org/10.1016/0016-7037(71)90127-X).
- Hercman H, Pawlak J, Gašiorowski M, Błaszczuk M, Sierpień P, Pruner P, Schnabl P, Kdýr Š, Matoušková Š, Zupan Hajna N, Mihevc A and Bosák P, submitted. Climate change at Matuyama/Brunhes magnetic reversal recorded in flowstone from the Račiška pečina Cave (Slovenia). *Palaeogeography, Palaeoclimatology, Palaeoecology*.
- Holden NE, 1990. Total half-lives for selected nuclides. *Pure and Applied Chemistry* 62(5): 941–958, DOI: [10.1351/pac199062050941](https://doi.org/10.1351/pac199062050941).
- Horáček I, Mihevc A, Zupan Hajna N, Pruner P and Bosák P, 2007. Fossil vertebrates and paleomagnetism update one of the earlier stages of cave evolution in the Classical Karst, Slovenia: Pliocene of Črnotiče II site and Račiška pečina. *Acta Carsologica* 37(3): 451–466, DOI: [10.3986/ac.v36i3.179](https://doi.org/10.3986/ac.v36i3.179).
- Imbrie J, Hays JD, Martinson DG, McIntyre A, Mix AC, Morley JJ, Pisias NG, Prell WL and Shackleton NJ, 1984. The orbital theory of Pleistocene climate: Support from a revised chronology of the marine $\delta^{18}\text{O}$ record. In: Berger A, Imbrie J, Hays H, Kukla G and Saltzman B, eds., *Milankovitch and Climate: Understanding the Response to Astronomical Forcing*. D. Reidel, Norwell: 269–305.
- Jaffey AH, Flynn KF, Glendenin LE, Bentley WC and Essling AM, 1971. Precision measurement of half-lives and specific activities of 235U and 238U. *Physical Review* C4: 1889–1906, DOI: [10.1103/PhysRevC.4.1889](https://doi.org/10.1103/PhysRevC.4.1889).
- Kolodny Y, Stein M and Machlus M, 2005. Sea-rain-lake relation in the Last Glacial East Mediterranean revealed by $\delta^{18}\text{O}$ – $\delta^{13}\text{C}$ in Lake Lisan aragonites. *Geochimica et Cosmochimica Acta* 69: 4045–4060, DOI: [10.1016/j.gca.2004.11.022](https://doi.org/10.1016/j.gca.2004.11.022).
- Krivic P, Bricelj M and Zupan M, 1989. Underground water connections in cicarije region and in middle Istra. *Acta Carsologica*, 18, Ljubljana, 265–295.

- Lachniet MS, 2006. Climatic and environmental controls on speleothem oxygen-isotope values. *Quaternary Science Reviews* 28(5): 412–432, DOI: [10.1016/j.quascirev.2008.10.021](https://doi.org/10.1016/j.quascirev.2008.10.021).
- Lachniet MS, 2009. Climatic and environmental controls on speleothem oxygen-isotope values. *Quaternary Science Reviews* 28(5–6): 412–432, DOI: [10.1016/j.quascirev.2008.10.021](https://doi.org/10.1016/j.quascirev.2008.10.021).
- Lambert WJ and Aharon P, 2011. Controls on dissolved inorganic carbon and $\delta^{13}\text{C}$ in cave waters from DeSoto Caverns: Implications for speleothem $\delta^{13}\text{C}$ assessments. *Geochemica et Cosmochimica Acta* 75: 753–768, DOI: [10.1016/j.gca.2010.11.006](https://doi.org/10.1016/j.gca.2010.11.006).
- Lascu I and Feinberg JM, 2011. Speleothem magnetism. *Quaternary Science Reviews* 30(23–24): 3306–3320, DOI: [10.1016/j.quascirev.2011.08.004](https://doi.org/10.1016/j.quascirev.2011.08.004).
- Lauritzen SE and Lundberg J, 1999. Speleothems and climate: a special issue of The Holocene. *The Holocene* 9: 643–647. DOI: [10.1191/095968399666229065](https://doi.org/10.1191/095968399666229065).
- Levin EN, Zipser JE and Cerling ET, 2009. Isotopic composition of waters from Ethiopia and Kenya: Insights into moisture sources for eastern Africa. *Journal of Geophysical Research Atmospheres* 114: 23, DOI: [10.1029/2009JD012166](https://doi.org/10.1029/2009JD012166).
- Lisiecki LE and Raymo ME, 2005. A Pliocene-Pleistocene stack of 57 globally distributed benthic $\delta^{18}\text{O}$ records. *Paleoceanography and Paleoclimatology* 20(1), PA1003, DOI: [10.1029/2004PA001071](https://doi.org/10.1029/2004PA001071).
- Lourens LJ, Hilgen FJ, Shackleton NJ, Laskar J and Gradstein D, 2004. *A Geologic Time Scale*. Cambridge University Press, 409–440.
- Mangini A, Spotl C and Verdes P, 2005. Reconstruction of temperature in the Central Alps during the past 2000 yr from a $\delta^{18}\text{O}$ stalagmite record. *Earth and Planetary Science Letters* 235: 741–751, DOI: [10.1016/j.epsl.2005.05.010](https://doi.org/10.1016/j.epsl.2005.05.010).
- McDermott F, Atkinson TC, Fairchild IJ, Baldini LM and Matthey DP, 2011. A first evaluation of the spatial gradients in $\delta^{18}\text{O}$ recorded by European Holocene speleothems. *Global and Planetary Change* 79: 275–287, DOI: [10.1016/j.gloplacha.2011.01.005](https://doi.org/10.1016/j.gloplacha.2011.01.005).
- McDermott F, Schwarcz H and Rowe PJ, 2006. Isotopes in speleothems In: Leng MJ, (ed.), *Isotopes in Palaeoenvironmental Research*. Springer, Dordrecht, The Netherlands, 185–226.
- McDermott F. 2004. Palaeo-climate reconstruction from stable isotope variations in speleothems: A review. *Quaternary Science Reviews* 23(7–8): 901–918. DOI: [10.1016/j.quascirev.2003.06.021](https://doi.org/10.1016/j.quascirev.2003.06.021).
- Mezga K, Urbanc J and Cerar S, 2014. The isotope altitude effect reflected in groundwater: A case study from Slovenia. *Isotopes in Environmental and Health Studies* 50(1): 33–51, DOI: [10.1080/10256016.2013.826213](https://doi.org/10.1080/10256016.2013.826213).
- Mickler PJ, Stern LA and Banner JL, 2015. Large kinetic isotope effects in modern speleothems. *Geological Society of America, Bulletin* 118(1–2): 65–81, DOI: [10.1130/B25698.1](https://doi.org/10.1130/B25698.1).
- Mihevc A, 2001. Speleogeneza Divaškega krasa. *ZRC Publishing*, Ljubljana.
- Mihevc A, 2007. The age of karst relief in West Slovenia. *Acta Carsologica* 36(1): 35–44, DOI: [10.3986/ac.v36i1.206](https://doi.org/10.3986/ac.v36i1.206).
- Milošević DD, Savić SM, Stankov U, Žiberna I, Pantelić MM, Dolinaj D and leščičen I, 2017. Maximum temperatures over Slovenia and their relationship with atmospheric circulation patterns. *Geografije* 122(1): 1–20, DOI: [10.37040/geografije2017122010001](https://doi.org/10.37040/geografije2017122010001).
- Moldovan OT, Mihevc A, Mikó L, Constantin S, Meleg I, Petculescu A and Bosák P, 2011. Invertebrate fossils from cave sediments: A new proxy for pre-Quaternary paleoenvironments. *Biogeosciences* 8: 1825–1837, DOI: [10.5194/bg-8-1825-2011](https://doi.org/10.5194/bg-8-1825-2011).
- Morinaga H, Yonezawa T, Adachi Y, Inokuchi H, Goto H, Yaskawa K, 1994. The possibility of inferring paleoseismicity from paleomagnetic dating of speleothems, western Japan. *Tectonophysics* 230(3–4): 241–248, DOI: [10.1016/0040-1951\(94\)90138-4](https://doi.org/10.1016/0040-1951(94)90138-4).
- Nehme C, Kluge T, Verheyden S, Nader F, Charalambidou I, Weissbach T, Gucl S, Cheng H, Edwards RL, Satterfield L, Eiche E, Claeys Ph, 2020. Speleothem record from Pentadactylos cave (Cyprus): new insights into climatic variations during MIS 6 and MIS 5 in the Eastern Mediterranean. *Quaternary Science Reviews* 250, DOI: [10.1016/j.quascirev.2020.106663](https://doi.org/10.1016/j.quascirev.2020.106663).
- Orland IJ, Bar-Matthews M, Ayalon A, Matthews A, Kozdon R, Ushikubo T and Valley JW, 2012. Seasonal resolution of Eastern Mediterranean climate change since 34 ka from a Soreq Cave speleothem. *Geochimica et Cosmochimica Acta* 89: 240–255, DOI: [10.1016/j.gca.2012.04.035](https://doi.org/10.1016/j.gca.2012.04.035).
- Pawlak J and Hercman H, 2016. Numerical correlation of speleothem stable isotope records using a genetic algorithm. *Quaternary Geochronology* 33: 1–12, DOI: [10.1016/j.quageo.2015.12.005](https://doi.org/10.1016/j.quageo.2015.12.005).
- Pruner P, Bosák P, Mihevc A, Kadlec J, Man O and Schnabl P, 2003. Preliminary report on palaeomagnetic research on Račiška pečina Cave, SW Slovenia. *11th International Karstological School „Classical Karst“. Karst Terminology*. Guide booklet of the excursions and abstracts of lectures or poster presentations, Postojna, July 2003: 35–37. Karst Research Institute ZRC SAZU, Postojna.
- Pruner P, Zupan Hajna N, Mihevc A, Bosák P, Man O, Schnabl P and Venhodová D, 2009. Magnetostratigraphy and fold tests from Račiška pečina and Pečina v Borštu caves (Classical Karst, Slovenia). *Studia Geophysica et Geodaetica* 54(1): 27–48, DOI: [10.1007/s11200-010-0002-1](https://doi.org/10.1007/s11200-010-0002-1).
- Róžański K, Araguas-Araguas L and Gonfiantini R, 1993. Isotopic patterns in modern global precipitation. *Climate Change in Continental Isotopic Records* 78: 1–36, DOI: [10.1029/GM078](https://doi.org/10.1029/GM078).
- Scholz D and Hoffmann D, 2008. $^{230}\text{Th}/\text{U}$ -dating of fossil corals and speleothems. *Quaternary Science Journal* 57(1–2): 52–76, DOI: [10.3285/eg.57.1-2.3](https://doi.org/10.3285/eg.57.1-2.3), 2008.
- Šikič D, Pleničar M and Sparica M, 1972. Osnovna geološka karta SFRJ, list Ilirska Bistrica, 1:100 000. Zvezni geološki zavod Beograd.

- Spötl C, Fohlmeister J, Cheng H and Boch R, 2016. Modern aragonite formation at near-freezing conditions in an alpine cave, Carnic Alps, Austria. *Chemical Geology* 435: 60–70, DOI: [10.1016/j.chemgeo.2016.04.017](https://doi.org/10.1016/j.chemgeo.2016.04.017).
- Sundqvist HS, 2007. Speleothems as environmental recorders: A study of Holocene speleothems and their growth environments in Sweden. WEB site: <<http://www.diva-portal.org/smash/get/diva2:190032/FULLTEXT01.pdf>>.
- Ünal-İmer E, Shulmeister J, Zhao JX, Uysal T and Feng YX, 2016. High-resolution trace element and stable/radiogenic isotope profiles of late Pleistocene to Holocene speleothems from Dim Cave, SW Turkey. *Palaeogeography, Palaeoclimatology, Palaeoecology*, 452: 68–79, DOI: [10.1016/j.palaeo.2016.04.015](https://doi.org/10.1016/j.palaeo.2016.04.015).
- Vaks A, Bar-Matthews M, Ayalon A, Matthews A, Frumkin A, Dayan U, Halicz L, Almogi-Labin A and Schilman B, 2006. Paleoclimate and location of the border between Mediterranean climate region and the Saharo–Arabian Desert as revealed by speleothems from the northern Negev Desert, Israel. *Earth and Planetary Science Letters* 249(3–4): 384–399, DOI: [10.1016/j.epsl.2006.07.009](https://doi.org/10.1016/j.epsl.2006.07.009).
- Vaks A, Woodhead J, Bar-Matthews M, Ayalon A, Cliff RA, Zilberman T, Matthews A and Frumkin A, 2013. Pliocene–Pleistocene climate of the northern margin of Saharan–Arabian Desert recorded in speleothems from the Negev Desert, Israel. *Earth and Planetary Science Letters* 368: 88–100, DOI: [10.1016/j.epsl.2013.02.027](https://doi.org/10.1016/j.epsl.2013.02.027).
- Van Couvering JA, 1996. *The Pleistocene Boundary and the Beginning of the Quaternary*. American Museum of Natural History, New York, DOI: [10.1017/CBO9780511585760](https://doi.org/10.1017/CBO9780511585760).
- Vreča P, Kanduč T, Žigon S and Trkov Z, 2005. Isotopic composition of precipitation in Slovenia in: Isotopic composition of precipitation in the Mediterranean Basin in relation to air circulation patterns and climate. Final report of a coordinated research project 2000–2004. International Atomic Energy Agency. IAEA-TECDOC-1453, WEB site: <https://www-pub.iaea.org/MTCD/publications/PDF/te_1453_web.pdf>.
- Wang P, Tian J and Lourens LJ, 2010. Stack of stable carbon and oxygen isotope record for Mediterranean Sea sediments. *Earth and Planetary Science Letters* 290(3–4): 319–330, DOI: [10.1594/PANGAEA.790006](https://doi.org/10.1594/PANGAEA.790006).
- Williams PW, Marshall A, Ford DC and Jenkinson AV, 1999. Palaeoclimatic interpretation of stable isotope data from Holocene speleothems of the Waitomo district, North Island, New Zealand. *The Holocene* 9: 649–657, DOI: [10.1191/095968399673119429](https://doi.org/10.1191/095968399673119429).
- Zacwijn WH, 1974. The Pliocene–Pleistocene boundary in western and southern Europe. *Boreas* 3(3): 75–97, DOI: [10.1111/j.1502-3885.1974.tb00666.x](https://doi.org/10.1111/j.1502-3885.1974.tb00666.x).
- Zupan Hajna N, Bosák P, Pruner P, Mihevc A, Hercman H and Horáček I, 2020. Karst sediments in Slovenia: Plio-Quaternary multi-proxy records. *Quaternary International* 546: 4–19, DOI: [10.1016/j.quaint.2019.11.010](https://doi.org/10.1016/j.quaint.2019.11.010).
- Zupan Hajna N, Mihevc A, Bosák P, Pruner P, Hercman H, Horáček I, Wagner J, Čermák S, Pawlak J, Sierpień P, Kdýr Š, Juříčková L and Švara A, 2021. Pliocene to Holocene chronostratigraphy and paleoenvironmental records from cave sediments: Račiška pečina section (SW Slovenia). *Quaternary International*, DOI: [10.1016/j.quaint.2021.02.035](https://doi.org/10.1016/j.quaint.2021.02.035).
- Zupan Hajna N, Mihevc A, Pruner P and Bosák P, 2008. Palaeomagnetism and magnetostratigraphy of karst sediments in Slovenia. *Carsologica* 8: 1–266, ZRC Publishing, Postojna–Ljubljana.
- Zupan Hajna N, Mihevc A, Pruner P and Bosák P, 2010. Palaeomagnetic research on karst sediments in Slovenia. *International Journal of Speleology* 39(2): 47–60, DOI: [10.5038/1827-806X.39.2.1](https://doi.org/10.5038/1827-806X.39.2.1).